Indian Journal of Chemistry
Vol. 55A, January 2016, pp. 9-15

Photocatalytic degradation of methylene blue and methyl violet using cation doped (Sn^{2+} and Ag^{+}) barium tellurite phosphate, $Ba_2TeO(PO_4)_2$

CH Sudhakar Reddy, Sreenu K, J R Reddy, G Ravi, Ravinder Guje, M Malathi & M Vithal*
Department of Chemistry, University College of Science, Osmania University, Hyderabad 500 007, India
Email: mugavithal@gmail.com

Received 14 October 2015; accepted 16 December 2015

One-dimensional barium tellurite phosphate of composition, $Ba_2TeO(PO_4)_2$, is prepared by solid state method. Tin (Sn^{2+}) and silver (Ag^{+}) doped $Ba_2TeO(PO_4)_2$ materials are prepared via a facile room temperature ion-exchange method. Structural, morphological, and optical properties of all the materials are characterized by powder X-ray diffraction, FT-IR, SEM-EDS, and UV-visible diffuse reflectance spectroscopy techniques. The band gap energy (E_g) of all the phosphates is deduced from their Kubelka–Munk (KM) plot. The synthesized phosphates are used as photocatalyst for the degradation of methylene blue and methyl violet dyes under the visible light irradiation. The systematic degradation pathways of the dyes are studied in the presence of all the photocatalysts and scavengers. The stability and reusability of all the photocatalyst are assessed by the cycling runs in the photodegradation experiment.

Keywords: Photocatalysts, Doping, Photodegradation, Dye degradation, Barium tellurite phosphate, Methylene blue, Methyl violet, Tin, Silver

Transition metal phosphates have been extensively investigated due to their rich structural chemistry and interesting properties[1-4]. The building blocks of such materials, viz., MO_6 octahedra (M = transition metal ion), PO_4 tetrahedra and/or $M'O_x$ (M' = alkali or alkaline earth) polyhedra, arrange in different ways leading to structural topologies like one-dimensional chains[5,6], two-dimensional layers[7-9], and three-dimensional tunnel structures[4,10-12]. These structural varieties have resulted in interesting properties such as high ionic conductivity[4,13-16], magnetic[17,18], catalytic[18], and second harmonic generating properties[19-21]. Further, if stereochemically active lone pair containing metal ion (such as Bi^{3+}, Te^{4+} or Pb^{2+}) is introduced into such lattices, variable coordination environments are possible leading to different structural topologies. It is reported that tellurium (Te^{4+}) containing phosphates exhibit different structures ranging from novel one-dimensional architectures to three-dimensional tunnel structures owing to the flexibility of tellurium coordination[7,22-25]. Barium tellurite phosphate, $Ba_2TeO(PO_4)_2$, having a novel one-dimensional chain structure has been studied by Ok & Halasyamani[26]. Its crystal structure, IR, Raman, UV-vis DRS, TGA, and dipole moment calculations are reported. The structure is characterized by chains made up of PO_4 and TeO_5 groups connected by P-O-Te and Te-O-Te bonds. The Te^{4+} ion is bonded to five oxygen atoms in a distorted square pyramidal geometry. Two TeO_5 units share edges to form Te_2O_8 dimers which are connected to PO_4 units. The two Ba^{2+} ions with 8- and 10-fold coordinations are present between the one-dimensional chains[26]. The ion exchange properties of $Ba_2TeO(PO_4)_2$ and the characterization resultant ion-exchanged materials, however, are not exploited despite having structurally convenient topology for ion exchange. It is well known that the optical and hence the catalytic properties of a material can be altered by doping with cations/anions in the lattice. In continuation of our search for better visible active photocatalysts for energy and environmental applications, attempts are made herein to vary the optical and catalytic properties of barium tellurite phosphates, $Ba_2TeO(PO_4)_2$ by exchanging Ba^{2+} with Ag^{+} and Sn^{2+} ions. To our knowledge the photocatalytic properties of $Ba_2TeO(PO_4)_2$ and its Ag^{+}/Sn^{2+} doped materials are not reported.

Materials and Methods

Preparation of Ag-$Ba_2TeO(PO_4)_2$ and Sn-$Ba_2TeO(PO_4)_2$ (ATOP and STOP)

Barium tellurite phosphate, $Ba_2TeO(PO4)_2$ (hereafter BTOP) was prepared by solid state method

as reported earlier[26]. Stoichiometric amounts of $Ba(NO_{3)2}$ (Merck-99%), TeO_2 (Aldrich-99.995%) and $NH_4H_2PO_4$ (SDFCL-99%) were ground in an agate mortar for one hour followed by heating at 650 °C/48 h with one intermittent grinding after 24 h. A white powder was obtained.

The parent BTOP was ion exchanged, with silver nitrate (SDFCL-99%) and tin chloride (SDFCL-99%) solutions, to prepare ATOP and STOP respectively. About.0.5 g of BTOP (0.82 mmol) was stirred with 100 mL each of $AgNO_3$ (3.94 mmol) (for ATOP) or acidified $SnCl_2$ (3.28 mmol) (for STOP) solutions at room temperature, separately. The stirring was continued for 24 h to ensure complete ion exchange. The color of the solutions changed to gray (ATOP) and light yellow (STOP). The resultant products after ion-exchange were washed with deionized water and dried in air at 80 °C for 12 h.

Characterization

The room temperature X-ray diffractograms of all samples were recorded using Rigaku MiniFlex 600 X-ray diffractometer (Cu Kα, λ = 1.5406 Å, 2θ = 10–55°, step size (2θ) = 0.02° and scan step time = 0.15 s) for phase confirmation. FT-IR spectra were recorded using Shimadzu spectrometer in the form of KBr pellets. The SEM-EDS images were recorded on a Hitachi SU-1500 variable pressure scanning electron microscope (VP-SEM). UV-vis spectrophotometer (Jasco V-650) was used for UV-vis diffuse reflectance spectra measurements in the range 200–900 nm. $BaSO_4$ was used as the reflectance standard.

Photocatalytic studies

The photocatalytic activity of all the samples was evaluated by photodegradation of methylene blue (MB) and methyl violet (MV) solutions using Heber visible annular type photo-reactor (model HVAR1234, Heber Scientific, India), under visible light irradiation using 300 W tungsten lamp as the light source. Aqueous MB solution (50 mL, initial conc.: C_0 = 1.0×10^{-5} mol/L) and MV solution (C_0 = 1.0×10^{-5} mol/L) were stirred with 0.05 g of catalyst separately in a cylindrical-shaped glass reactor at room temperature in air. The suspensions were stirred in the dark for an hour to establish adsorption-desorption equilibrium. Then the solutions were exposed to light with continuous stirring. At regular 30 min intervals, about 3 mL of solution was collected and centrifuged to remove the catalyst particles. The change in the concentration of MB (or MV) was obtained by recording the absorbance at 664 (or 580) nm using a UV-vis spectrophotometer. Similar experiments were repeated by using scavengers (Isopropanol, Ammonium oxalate, and Benzoquinone) for testing for the presence of oxidative species. The reaction mixture consisted of 3 mL of 2 m*M* scavenger, 47 mL of MB (or MV) and 0.05 g of the catalyst.

Results and Discussion

The parent BTOP was prepared by a facile solid state method while ion exchange method was adopted for the preparation of Ag- and Sn-doped BTOP. All the prepared materials were subjected to powder X-ray diffraction (XRD) for phase characterization. The powder XRD patterns of BTOP, ATOP, and STOP are shown in Fig. 1. The powder pattern of parent BTOP is free from impurities and in agreement with reported data[26]. It is crystallized in the triclinic lattice with the P1 space group. The intensities of diffraction lines (*d*-lines) of all three samples are fairly large with insignificant background indicating high crystallinity. The XRD patterns of doped samples, ATOP and STOP, are similar to that of BTOP and free from impurities. However, when the powder patterns are plotted in the expanded scale (Fig. 1, inset) a shift in *d*-lines is detected for silver and tin doped samples compared to the parent material. The *d*-lines of ATOP and STOP are shifted to lower 2θ values compared to that of BTOP. The ionic radii of Ag^+ (1.14 Å) and Sn^{2+} (1.27 Å) are smaller than that of Ba^{+2} (1.60 Å). Therefore substitution of Ba^{2+} by Sn^{2+} (or Ag^+) should in principle lead to lower unit cell parameters and hence

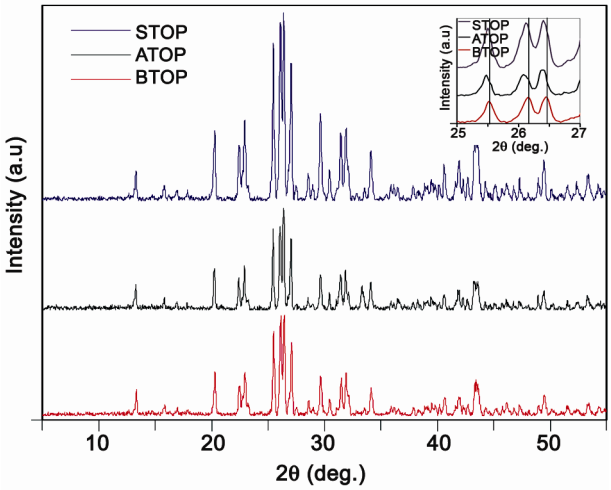

Fig. 1–Powder X-ray diffraction patterns of BTOP, ATOP and STOP.

d-lines should shift to higher 2θ values. However, experimentally, the *d*-lines have been shifted to lower 2θ values. The possible reason could be the incorporation of water into BTOP lattice during ion exchange process which is substantiated in the next section. Both ATOP and STOP also crystallized in the triclinic lattice with P1 space group and are isomorphous with the parent BTOP.

We have recorded the FT-IR spectra of all the samples in the region 400–4000 cm^{-1} to observe the vibration modes of Te-O, P-O, Te-O-P, and O-H bonds (Fig. 2 (a, b)). It is observed that the IR spectra of all the samples are similar and comparable with that reported for $Ba_2TeO(PO_4)_2$[26]. Compared to the parent BTOP, ATOP, and STOP show additional broad vibrational band in the region around 3000–3600 cm^{-1}, which can be ascribed to the stretching vibration modes of O-H. The rest of the vibration bands in the region (i) 650–880 and 430 cm^{-1} (ii) 950–1150 and 450–570 cm^{-1} and (iii) 600cm^{-1} are attributed to stretching modes of Te-O, P-O, and Te-O-P, respectively[7,27-28].

The optical properties of BTOP, ATOP and STOP were examined using UV-vis diffuse reflectance spectroscopy. The absorption and diffused reflectance spectra of all the samples are shown in Fig. 3. Accurate band gap energy (E_g) of all the phosphates can be obtained from the Kubelka-Munk (KM) plot, $(Khv)^{1/2}$ versus hν, where *K* is the reflectance transformed according to Kubelka-Munk [$K= (1-R)^2/2R$, where *R* is reflectancy (in %)] and *hv* is the photon energy. Extrapolation of the linear portion of the plot to $(Khv)^{1/2} = 0$ (i.e. to the x-axis) gives an estimation of the band gap energy. The

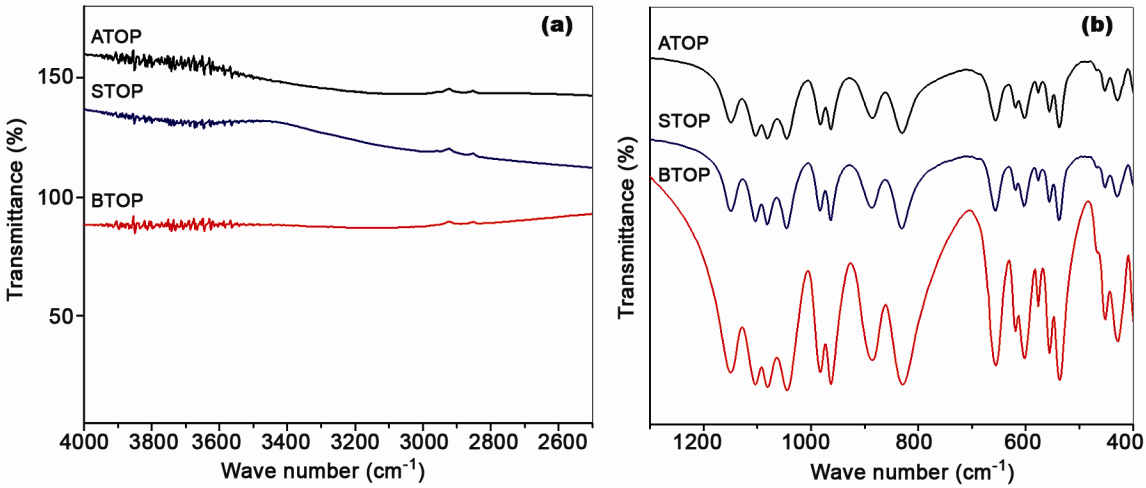

Fig. 2–FT-IR spectra of BTOP, ATOP, and STOP in the (a) 4000–2500 and (b) 1300–400 cm^{-1} regions.

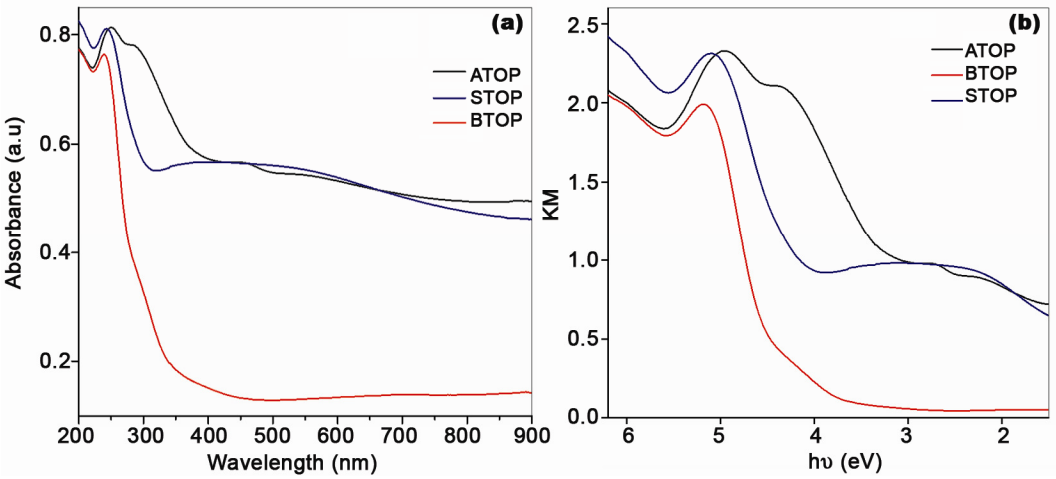

Fig. 3–(a) UV-vis absorption and (b) diffused reflectance spectra of BTOP, ATOP and STOP.

diffused reflectance spectrum of BTOP shows absorption edge at 342 nm corresponding to band gap energy consistent with reported data, i.e., 3.62 eV[26]. The diffused reflectance spectras of ATOP and STOP show absorption edge at 522 and 450 nm leading to a band gap of 2.37 and 2.75 eV, respectively.

The morphology and elemental composition of all the samples (BTOP, ATOP, and STOP) were obtained by scanning electron microscopy and energy dispersive spectroscopy respectively. The SEM images and EDS of BTOP, ATOP, and STOP are shown in Fig. 4. From the SEM images, it is clear that the morphology of all the samples was similar and observed as unspecified bunch like agglomeration. The energy dispersive spectra of ATOP is characterized by peaks corresponding to Ag, Te, P, and O. Similarly, peaks belonging to elements Sn, Te, P, and O are observed for STOP. The absence of the peak belonging to Ba in the energy dispersive spectra of ATOP and STOP indicates 100% exchange of Ba^{2+} by Ag^{+} and Sn^{2+} respectively.

Photocatalytic activity

The photocatalytic activities of BTOP, ATOP, and STOP were examined against the photodegradation of MB and MV aqueous solutions under visible light illumination. The concentration of MB (or MV) was monitored by measuring its absorbance at 664 nm (580 nm) and by recording the UV-vis spectra. The temporal changes in the concentrations of MB and MV in the presence and absence of all the catalysts are shown in Figs 5 and 6, respectively. From Fig. 5, it is obvious that the concentration of MB decreases with increase in irradiation time of visible light in the presence of all catalysts. A blank experiment without catalyst shows about 23% of MB degradation after 180 min of visible light irradiation. The percentage of MB degradation in the presence of BTOP, ATOP and STOP during the same time period is found to be 51%, 91%, and 78%, respectively. The photolysis of MV, on the other hand, is about 10% in 180 min of visible light irradiation. The photodegradation of MV in the presence of the catalysts BTOP, ATOP and

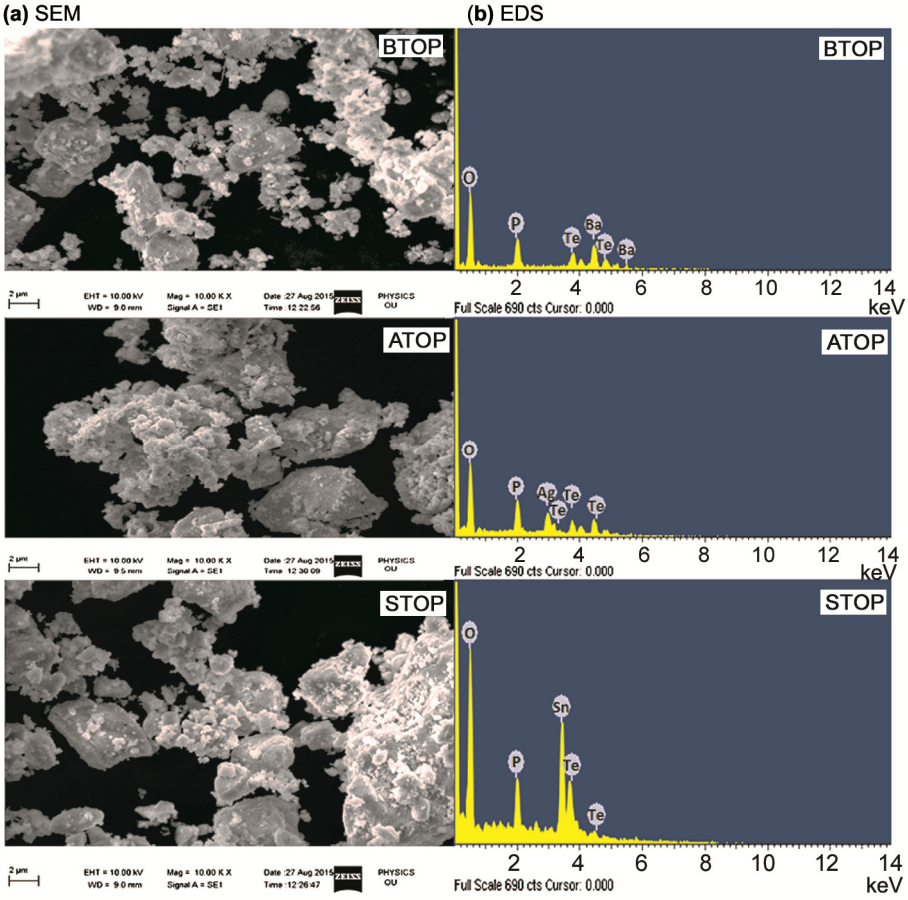

Fig. 4–(a) SEM and (b) EDS of BTOP, ATOP and STOP.

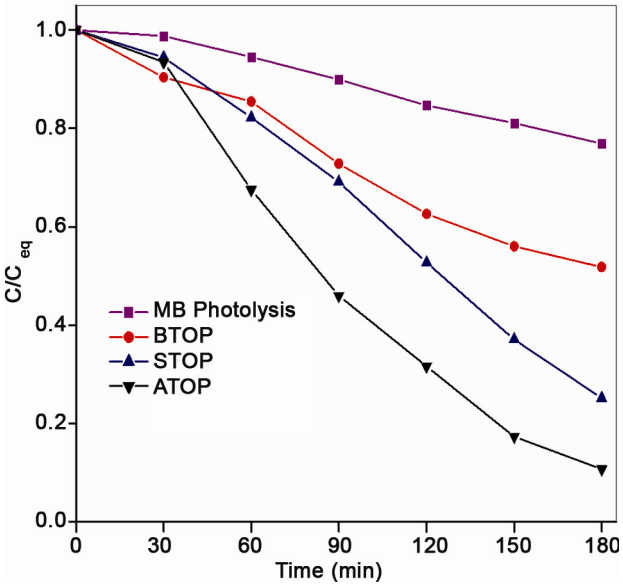

Fig. 5–Photodegradation curves of methylene blue solution under visible light irradiation over BTOP, ATOP and STOP.

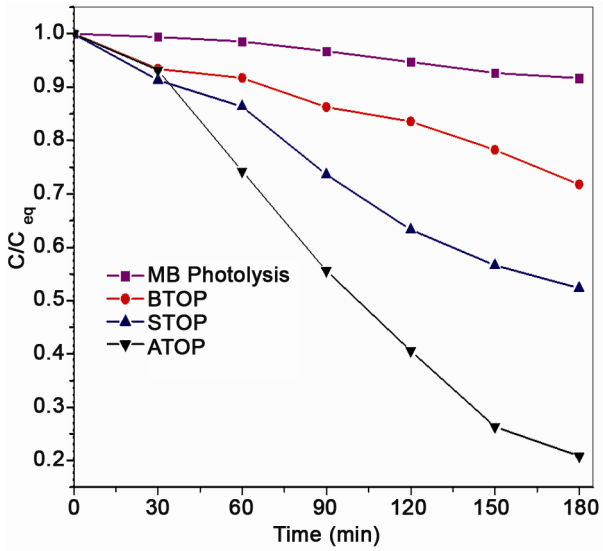

Fig. 6–Photodegradation curves of methyl violet as a function of irradiation time over BTOP, ATOP and STOP.

STOP is found to be 32%, 82%, and 51%, respectively after 180 min of visible light irradiation. The percentage of dye degradation in the presence of catalysts is higher compared to blank experiments. Therefore, the higher percentage of MB/MV degradation can be attributed to a combined effect of catalysts and visible light irradiation. A comparison of the photoactivity of the catalysts with reference to the chemical nature of catalysts and band gap energy has been attempted. Both Ag^{+} and Sn^{2+} doped $Ba_2TeO(PO_4)_2$ show higher photoactivity than the parent $Ba_2TeO(PO_4)_2$ in the degradation of MB/MV. The band gap energy of the three catalysts follows the order: BTOP (3.62 eV) > STOP (2.75 eV) > ATOP (2.37 eV). Lower band gap energy implies absorption of more photons leading to a higher number of electron-hole pairs. Thus, it is expected that the photocatalytic activity of these catalysts shall follow the order: ATOP > STOP > BTOP as observed experimentally. It is well-known that the photocatalytic activity of a catalyst depends on factors such as surface structure, extent of crystallinity, surface area, structure, bandgap energy of the catalyst, and the adsorption ability of the pollutant. In the present study, the higher photocatalytic activity observed for the doped materials (ATOP and STOP) may be due to their lower band gap energy and relatively higher number of electron-hole pairs generated.

The decolorisation of organic dye on the surface of a catalyst is primarily initiated by illumination of light of energy equal to or greater than the band gap energy of the catalyst. This results in the formation of charge carriers, viz., conduction band electron and valence band hole. Both electrons and holes participate in a series of redox reactions to degrade the organic dye into simple molecules. The efficiency of a catalyst depends on the photo-induced electrons. The photo-induced electron may (i) recombine with holes with or without radiative emission, or (ii) be trapped by a defect, or (iii) react with adsorbed/dissolved oxygen to form $O_2^{\bullet -}$. Of these, only the last process leads to degradation of organic dyes. The holes in the valence band may react with surface OH^{-} ions to form reactive $^{\bullet}OH$ species or may directly react with dye molecule leading to its degradation. To examine the precise role of these reactive species ($^{\bullet}OH$, $O_2^{\bullet -}$, and h^{+}) in the photodegradation of MB and MV, additional experiments were carried out under identical conditions in the presence of scavengers such as ammonium oxalate (AO), benzoquinone (BQ), and isopropyl alcohol (IPA) for quenching the holes, h^{+}, $O_2^{\bullet -}$, and $^{\bullet}OH$ respectively[29-31]. The variation of concentration of MB (or MV) in the presence of ATOP and scavengers is displayed in Figs 7 and 8. It can be seen from Fig. 7 that the extent of degradation of MB is reduced from 91% (without scavenger) to 27%, 32%, and 34% in the presence of AO, BQ, and IPA respectively. Thus, it is confirmed that all the three reactive species (h^{+}, $O_2^{\bullet -}$, and $^{\bullet}OH$) have participated in the degradation of MB.

Similar results were obtained in the degradation of MV in the presence of ATOP and scavengers (Fig. 8). Therefore, it can be concluded that h^+, $O_2^{\bullet -}$, and $^{\bullet}OH$ have actively participated in the degradation of MB and MV.

From the above results, the probable photocatalytic degradation pathway is given in Scheme 1.

$$\text{Catalyst (ATOP)} + h\nu \rightarrow e_{cb}^- + h_{vb}^+$$
$$H_2O + h_{vb}^+ \rightarrow {}^{\bullet}OH + H^+$$
$$O_2 + e_{cb}^- \rightarrow O_2^{\bullet -}$$
$$O_2^{\bullet -} + H^+ \rightarrow HO_2^{\bullet}$$
$$2HO_2^{\bullet} \rightarrow H_2O_2 + O_2$$
$$H_2O_2 \rightarrow 2OH^{\bullet}$$
$$^{\bullet}OH, O_2^{\bullet -}, h_{vb}^+ + \text{Dye (MB/MV)} \rightarrow \text{Byproducts}$$

Scheme 1

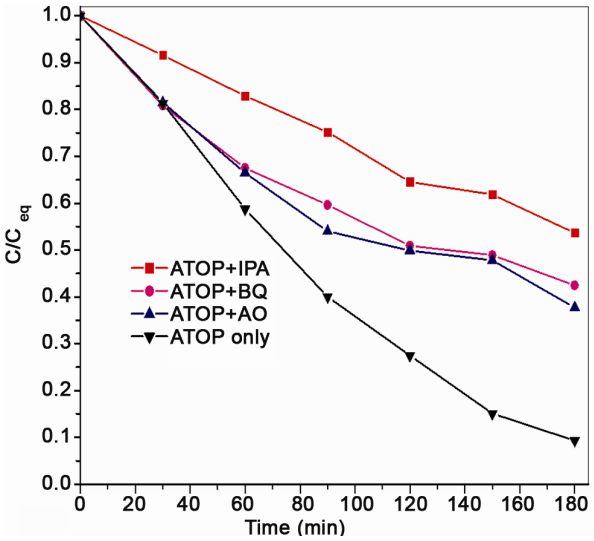

Fig. 7–Photodegradation of methylene blue in presence of ATOP and scavengers.

The practical applications of a photocatalyst are dependent on its stability during the photoreaction. In the present investigation, the photocatalysts were reused for four times for MB and MV degradation. Figures 9a and 9b show the photodegradation of MB and MV using ATOP as a photocatalyst. It is observed that the photocatalyst, ATOP, exhibits almost the same activity for photodegradation of both MB and MV in all the four cycles. This confirms that the structure/composition of the ATOP remains the same even after the fourth cycle of photodegradation. Thus, ATOP can be considered as an attractive photocatalyst for industrial waste/pollutant purification.

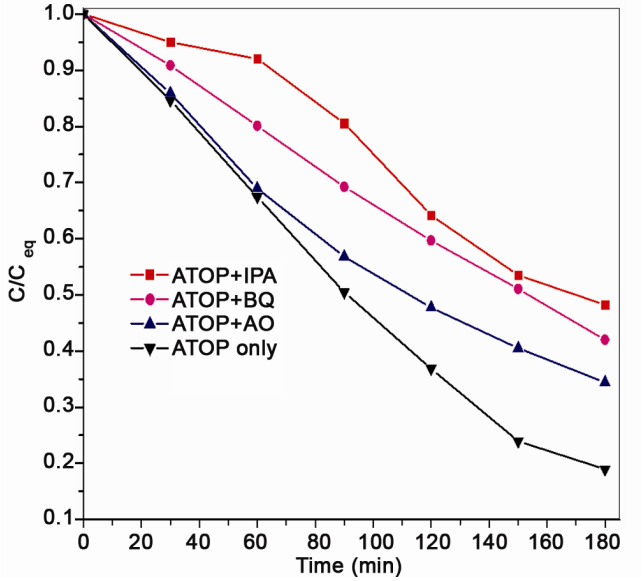

Fig. 8–Photodegradation of methyl violet in presence of ATOP and scavengers

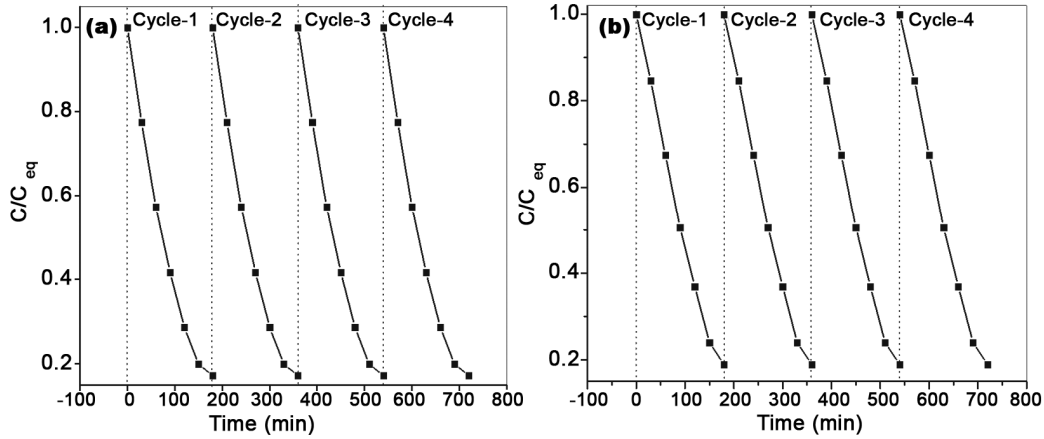

Fig. 9–(a, b) Cycling runs in the photocatalytic degradation of methylene blue and methyl violet aqueous solutions in the presence of ATOP.

Conclusions

Parent BTOP was prepared by a facile solid state method while ion exchange method was adopted for the preparation of Ag^+- and Sn^{2+}-doped BTOP. Both Ag^+- and Sn^{2+}-doped BTOP (i.e., ATOP and STOP) are isomorphous with parent BTOP and crystallize in the triclinic lattice with the P1 space group. The vibrational bands observed for ATOP and STOP are similar and comparable with the bands of the parent BTOP. The ion exchange was confirmed by shift in the d-lines, absence of Ba and presence of Ag and Sn peaks in their EDS. The Ag^+ and Sn^{2+}substitution for Ba^{2+} in BTOP is quite effective in decreasing the band gap energy and increasing the photocatalytic activity. The diffused reflectance spectra of BTOP, ATOP, and STOP show absorption edge at 342, 522, and 450 nm leading to the band gap of 3.61, 2.37, and 2.75 eV, respectively. The photoactivity of the catalysts in the degradation of MV and MB follow the order: BTOP < STOP < ATOP. The photocatalytic experiments in the presence of radical quenchers confirm that $^{\bullet}O_2^-$, $^{\bullet}OH$, and h^+ are the main reactive species in the photocatalytic degradation mechanism of MB and MV under visible light irradiation. All the photocatalysts were found to be chemically stable and can be used up to at least four cycles for the photodegradation of MB and MV.

Acknowledgement

The authors acknowledge the assistance of Department of Science & Technology (DST), New Delhi, India, under PURSE and FIST schemes, and, University Grants Commission, New Delhi, India, under UPE program.

References

1 Goodenough J B, Hong H Y P & Kafalas J, *Mater Res Bull*, 11 (1976) 203.
2 Knauth P, *Solid State Ionics*, 180 (2009) 911.
3 Anantharamulu N, Rao K K, Rambabu G, Kumar B V, Radha V & Vithal M, *J Mater Sci*, 46 (2011) 2821.
4 Wang E & Greenblatt M, *Chem Mater,* 3 (1991) 542.
5 Borel M M, Leclaire A, Chardon J, Michel C, Provost J & Raveau B, *J Solid State Chem*, 135 (1998) 302.
6 Zid M F, Jouini T & Jouini N, *C R Acad Sci, Sec IIc: Chim,* 309 (1989) 343.
7 Ok K M, Orzechowski J & Halasyamani P S, *Inorg Chem,* 43 (2004) 964.
8 Hoareau T, Leclaire A, Borel M M, Grandin A & Raveau B, *J Solid State Chem*, 116 (1995) 87.
9 Borel M M, Leclaire A, Chardon J, Provost J & Raveau B, *J Solid State Chem*, 137 (1998) 214.
10 Lang B, Ziebarth B & Elsasser C, *Chem Mater*, 27 (2015) 5040.
11 Yvoire F D, Pintard-Screpel M, Bretey E & Rochere M, *Solid State Ionics,* 9–10 (1983) 851.
12 Berry F J & Vithal M, *Polyhedron,* 14 (1995) 1113.
13 Wang E & Greenblatt M, *Chem Mater,* 3 (1991) 703.
14 Rambabu G, Anantharamulu N, KoteswaraRao K, Prasad G & Vithal M, *Mater Res Bull*, 43 (2008) 1509.
15 Arbi K, Mandal S, Rojo J M & Sanz J, *Chem Mater,* 14 (2002) 1091.
16 Kamaya N, Homma K, Yamakawa Y, Hirayama M, Kanno R, Yonemura M, Kamiyama T, Kato Y, Hama S, Kawamoto K & Mitsui A, *Nat Mater*, 10 (2011) 682.
17 Das B B, Benhamada L, Grandin A, Borel M M, Leclaire A & Raveau B, *Mater Chem Phys,* 39 (1995) 239.
18 Boudin S, Guesdon A, Leclaire A & Borel M M, *Int J Inorg Mater*, 2 (2000) 561.
19 Tordjman I, Masse R & Guitel J C, *Z Kristallogr*, 139 *(*1974) 103.
20 Liang C S, Harrison W T A, Eddy M M, Gier T E & Stucky G D, *Chem Mater*, 5 (1993) 917.
21 Gopalakrishnan J, Ramesha K, Kasthuri Rangan K & Pandey S, *J Solid State Chem*, 148 (1999) 75.
22 Mayer H*, Z Kristallogr*, 141 (1975) 354.
23 Alcock N W & Harrison W D*, Acta Crystallogr B*, 38 (1982) 1809.
24 Mayer H & Pupp G*, Z Kristallogr*, 145 (1977) 321.
25 Guesdon A & Raveau B, *Chem Mater,* 12 (2000) 2239.
26 Ok K M & Halasyamani P S, *J Solid State Chem*, 179 (2006) 1345.
27 Belik A A, Izumi F, Azuma M, Kamiyama T, Oikawa K, Pokholok K V, Lazoryak B I & Takano M, *Chem Mater*, 17 (2005) 5455.
28 Tomaszewski P E, Mączka M, Majchrowski A, Waśkowska A & Hanuza J, *Solid State Sciences*, 7 (2005) 1201.
29 Reddy J R, Ravinder G, Kumar V N, Shrujana P, Radha V & Vithal M, *J Alloys Comp*, 618 (2015) 815.
30 Zhang N, Zhang Y, Yang M Q, Tang Z R & Xu Y J, *J Catal*, 299 (2013) 210.
31 Xu Y S & Zhang W D, *Dalton Trans*, 42 (2013) 1094.